16th World Conference on Earthquake, 16WCEE 2017

Santiago Chile, January 9th to 13th 2017

Paper N° 875 (Abstract ID)

Registration Code: S-W1461893314

DEFORMATION CAPACITY OF FLANGE-WELDED WEB-BOLTED MOMENT CONNECTION UNDER CYCLIC LOADING

K. Takatsuka[1], K. Suita[2] and T. Umeda[3]

[1] *Assistant Professor, Kyoto University Japan, takatsuka@archi.kyoto-u.ac.jp*
[2] *Professor, Kyoto University Japan, suita@archi.kyoto-u.ac.jp*
[3] *Former Graduate Student, Kyoto University Japan, t-umeda@jfe-steel.co.jp*

Abstract

Recent advances in seismology have enabled the precise prediction of long-period ground motions produced by ocean-trench earthquake, such as the Nankai trough earthquake in Japan. Long-period ground motions cause significant cyclic deformation to moment connections in the plastic range, which may lead to fracture. Most steel buildings in Japan are constructed using rolled hollow section columns and wide flange beams, and beam flanges are connected by CJP groove weld and a beam web is connected by bolts to column. If the web-bolted connection has insufficient flexural strength, as commonly designed in early days, deformation capacity of the moment connection decreases and possibility of fracture will increase. In the previous researches, deformation capacity under cyclic loading was usually estimated by Miner rule based on the concept of fatigue. However, previous experimental studies indicated that Miner rule is inaccuracy of estimation.

The objective of this study is to investigate the effect of flexural strength of beam web connection on deformation capacity before fracture of beam flange due to cyclic loading. Two types of moment connections using weld access hole details, one is flange-welded web-bolted moment connection and the other is flange and web-welded moment connection, were prepared for test specimens. Three types of cyclic loadings, i.e. constant amplitudes, two-step constant amplitudes and random amplitudes were tested.

Deformation capacity was compared by constant amplitude cyclic loading with respect to loading amplitudes. From the relationship between loading amplitude and the number of cycles until fracture, deformation capacity of web-welded specimens is larger than that of web-bolted specimens and the difference becomes obvious at larger loading amplitude. From the comparison of the bending moment carried by the beam flange and the beam web, the bending moment carried by the beam flange is larger after slippage of the bolted web connection.

The fracture of moment connection under varying amplitude loading was estimated. In previous research, we conducted varying amplitude loading tests for welded moment connections and proposed a method to estimate deformation capacity using the formulated crack propagation at the weld considering the effect of loading amplitude and welding details. In this study, a total four cyclic loading tests by two kinds of two-step amplitude, i.e. increasing amplitude and decreasing amplitude, and a total of four cyclic loading tests by two kinds of random amplitude simulating seismic responses by long-period ground motion were conducted.

From the results of two-step amplitude loading tests, it is shown that the deformation capacity under decreasing amplitude loading is larger than increasing amplitude loading and this phenomenon is estimated by the proposed estimation method. From the results of random amplitude loading tests, it is also shown that the proposed estimation method well evaluate the instant of fracture and the accuracy of the method is better than Miner rule.

Keywords: Moment Connection; Deformation Capacity; Cyclic Loading; Flexural Strength; Crack Propagation

1. Introduction

Recent advances in seismology have enabled the precise prediction of long-period ground motions produced by ocean-trench earthquakes, such as the Nankai Trough earthquake in Japan. The characteristics of these ground motions are different from those of conventional strong motion of fault-associated earthquakes such as El Centro 1940 and Taft 1952. Because the periods of ground motion for ocean-trench earthquakes are longer than two seconds and the duration can be up to ten minutes, tall buildings are strongly shaken; a well-known example of this is the Great East Japan Earthquake (Kasai et al.[1]). Furthermore, long-period ground motions cause significant cyclic deformation to moment connections in the plastic range, which may lead to fracture (Suita[2]).

Most steel buildings in Japan are constructed by rolled hollow section columns and wide flange section beams, and the beam-to-column connections are welded through-diaphragm type. In case the connection is shop-weld, moment connection is fabricated with weld access holes and beam web is connected by a fillet weld, whereas in case the connection is field-weld, moment connection contained no weld access hole and beam web is connected by high-tension bolts with sheer plate. These welded details are recommended in the Japanese Architectural Standard Specification (JASS 6[3]) as shown in Figs. 1.

In the design of field-welded moment connections before 1970s in Japan, shear force is regarded to be carried by only the web bolted-connection and bending moment is carried by flange-welded connection; therefore, slippage of web connection caused by insufficient flexural strength decreases the deformation capacity of moment connections. In addition, steel columns in Japan are often using box-shaped section; excessive out-of-plane deformation of columns connected to beam webs also decreases the deformation capacity of the moment connections, whereas little out-of-plane deformation occurs when the column has sufficient thickness and is connected to a beam flange by a diaphragm plate. Therefore, the calculation method of necessary flexural strength of the moment connection considering the out-of-plane deformation was proposed by Suita and Tanaka[4].

Whereas, even if a welded moment connection – with or without a weld access hole – is designed to according to the recommendation, repeated plastic deformation can still result in fracture. Campbell et al.[5],[6] and Amiri et al.[7] conducted cyclic loading tests for beam-to-column connections and time-history analysis, and investigated the deformation capacity based on Miner's rule (Miner[8]) or the Coffin-Manson rule (Coffin[9] and Manson[10]). These previous studies estimated fracture using cumulative deformation; however, Zhou et al.[11] and Yamada et al.[12] demonstrated that the deformation capacity differs according to the loading history.

To avoid fracture of moment connections fabricated by using conventional Japanese connection with weld access holes during cyclic loading, it is important to investigate the effect of flexural strength of the connection on the deformation capacity. In this paper, two types of specimen with different web connections were prepared for loading tests. Constant-amplitude cyclic loading tests were conducted and a method was developed to evaluate damage and the deformation capacity of welded moment connections subjected to seismic response. To calculate the cumulative damage, the crack propagations in the vicinity of the beam flange connection was closely observed and analyzed as a function of the number of cycles. The validity of the proposed method was verified by comparing the results of two different constant-amplitude tests and random amplitude tests. In addition, referring the previous test results of cyclic loading by Suita et al.[13] for the specimen fabricated without weld access holes, the effect of weld access holes on deformation capacity was also investigated.

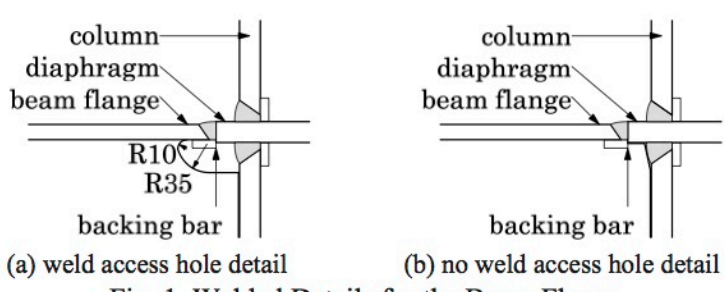

Fig. 1. Welded Details for the Beam Flange

2. Steel Moment Connection Specimen

The test specimens were beam-to-column sub-assmblages, as shown in Figs. 2. The beam was a wide flange section (H–500×200×10×16) of SN490B steel and the column was a cold formed square hollow section (RHS-350×350×22) of BCR295 steel. The beam-to-column connection was through- diaphragm type and was shop-welded. The beam flange was connected by a complete-joint- penetration (CJP) groove weld to the diaphragm plate (22mm thickness, SN490C) with weld access holes. Three types of moment connection were tested. The beam web of SCS was connected by a fillet weld, and the beam web of SCWB was connected by high-tension bolts with sheer plate. Whereas, the connection of NSS was fabricated without weld access holes.

The yield and tensile strength and elongations of the steels used for the test specimens obtained from tensile coupon tests are summarized in Table 1, and the flexural strengths are summarized in Table 2. The beam and column sections were determined in order to keep the column and panel zone in the elastic range even after the beam reaches the ultimate flexural strength. Three rib stiffeners were placed in the vicinity of the beam end in all specimens to prevent local buckling of the beam flange and web.

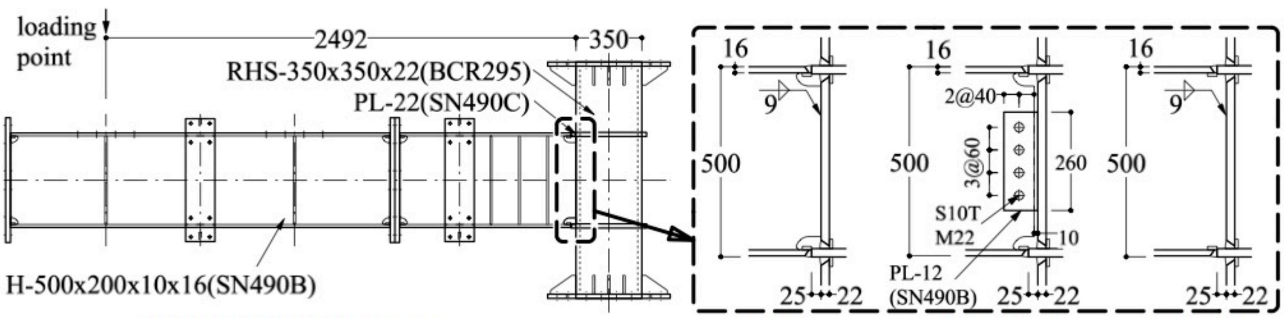

(a) Shape of Test Specimen (b) SCS (c) SCWB (d) NSS

Fig. 2. Test Specimen (unit: mm)

Table 1. Material Properties of the Test Specimen (SCWB)

Element	Steel grade	σ_y [N/mm^2]	σ_u [N/mm^2]	ε_u [%]
Beam flange	SN490B	352	525	26.0
Beam web	SN490B	386	540	21.8
Column	BCR295	393	441	23.1
Shear Plate	SN490B	366	531	23.1

*σ_y: Yield stress, σ_u: Tensile strength, ε_u: Elongation

Table 2. Flexural Strength of the Moment Connection

Specimen	${}_bM_p$ [kN·m]	m	${}_jM_{fu}$ [kN·m]	${}_jM_{wu}$ [kN·m]	${}_jM_u$ [kN·m]	${}_jM_u$ / ${}_bM_p$
SCS	728	0.899	790	185	975	1.34
SCWB	739	0.431	800	45.6	846	1.14
NSS	740	1.000	819	214	1033	1.40

*${}_bM_p$: Plastic moment, m: Non-dimensional flexural strength of beam web connection,

${}_jM_{fu}$: Flexural strength of beam flange connection, ${}_jM_{wu}$: Flexural strength of beam web connection,

${}_jM_u$: Flexural strength of beam connection

3. Constant Amplitude Loading Test

3.1 Test Program

The setup for the loading tests is shown in Fig. 3. The column ends were connected to column stubs, which were fastened to pin supports. Two sets of lateral supports were placed on the beam to restrict out-of-plane deformation. The beam end was clamped to a dynamic actuator at a distance of 2.667m from the centerline of the column.

The loading amplitude was determined from the ductility of beam rotation ($\mu = \theta/\theta_p$, where θ is the beam rotation), as shown in Fig. 4(a), and θ_p is the elastic component of θ corresponding to the full plastic moment of the beam, ${}_bM_p$, at the face of the column, as shown in Fig. 4(b). Loading tests were conducted at three different rotation amplitudes (μ = 1.2, 2.0 and 3.0).

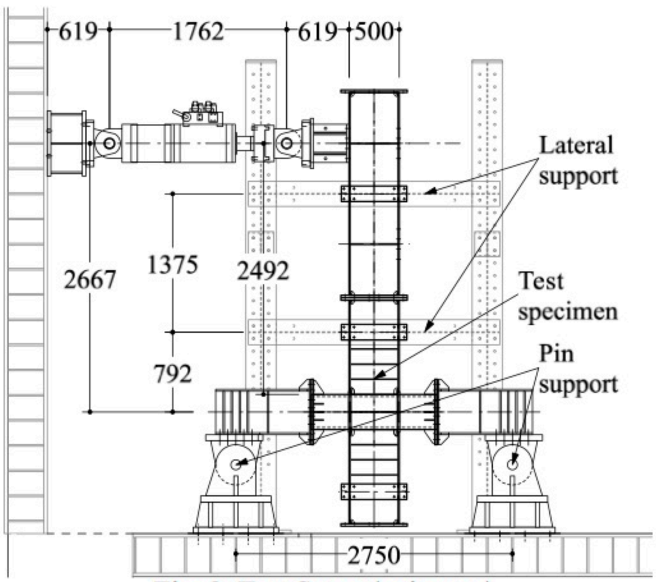

Fig. 3. Test Setup (unit: mm)

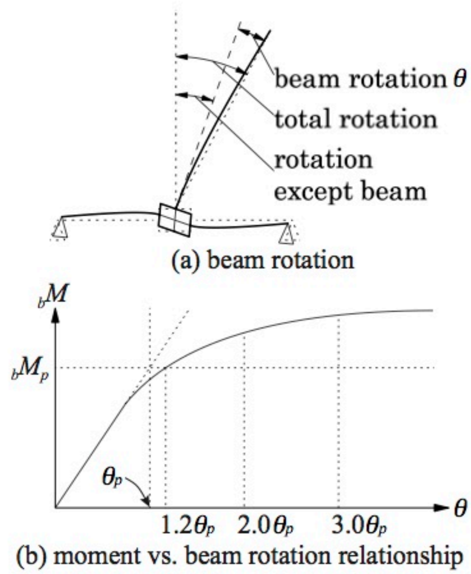

Fig. 4. Loading Amplitude

3.2 Test Results

The relationship between the bending moment, ${}_bM/{}_bM_p$, and the rotation of the beam, θ/θ_p, is shown in Figs. 5, and the result of all tests are summarized in Table 3. In this study, the cumulative plastic deformation η_F is estimated as the sum of the plastic deformation before fracture divided by θ_p.

Both SCS and SCWB specimens started to fail, as indicated by the formation of two cracks, after a certain number of cycles. One crack initiated at the toe of the weld access hole and the other initiated at the beam flange sides of the bond of the CJP weld at either the start or end of the welding line. The former crack propagated in the thickness direction of the beam flange and the latter crack propagated along the weld line with gradually increasing propagation rate. After the former crack penetrated the beam flange, both cracks joined and resulted in fracture. Examples of the fracture of the SCS and SCWB specimens are shown in Figs. 6.

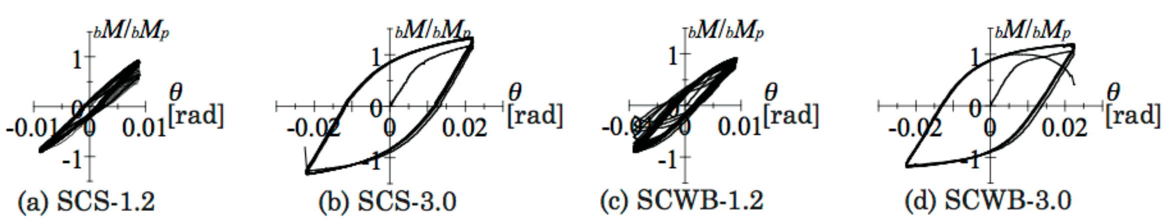

Fig. 5. Relationship between the Moment and Rotation Obtained from Constant Amplitude Loading Tests

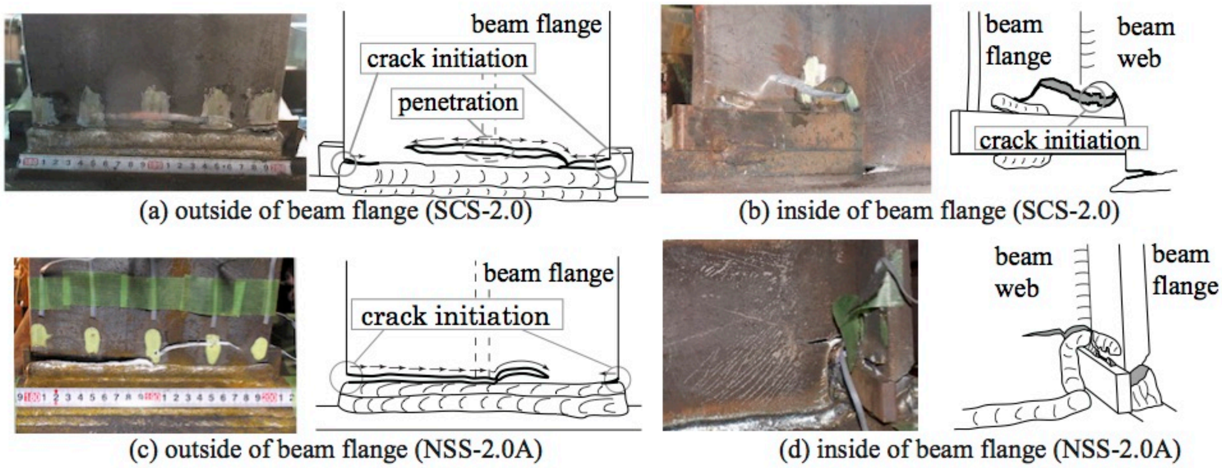

Fig. 6. Examples of Fracture of the Beam Flange

Table 3. Summary of Results from Constant-Amplitude Loading Tests

Test name	**Peak Bending Moments**		**Number of Cycle before fracture N_F [cyc]**	**Cumulative Plastic Deformation before fracture η_F**
	$M_{max}/_bM_p$	**$M_{min}/_bM_p$**		
SCS-1.2a	0.941	0.927	265	189
SCS-1.2b	0.920	0.937	256	178
SCS-2.0	1.19	1.18	30	92.0
SCS-3.0	1.34	1.32	9	58.2
SCWB-0.8	0.734	0.740	531	110
SCWB-1.2	0.915	0.905	119	115
SCWB-2.0	1.09	1.09	23	77.1
SCWB-3.0	1.14	1.18	7	45.7

3.3 Effect of Flexural Strength on Deformation Capacity

The relationship between the maximum bending moment, $M_{max}/_bM_p$, and the ductility amplitude, $\mu = \theta / \theta_p$, obtained from constant-amplitude loading tests is shown in Fig. 7. The $M_{max}/_bM_p$ of SCS obtained from the test results are larger than that of SCWB, which corresponds to the order of the calculated flexural strength, $_jM_u$.

The relationship between the number of cycles until fracture, N_F, and the ductility amplitude μ are shown in Fig. 8 in the form of a double logarithmic plot. The linear relationships obtained from regression analysis are expressed in Eqs. 1.

$$\text{SCS:} \quad N_F = 493\mu^{-3.75} \tag{1a}$$

$$\text{SCWB:} \quad N_F = 236\mu^{-3.27} \tag{1b}$$

$$\text{NSS:} \quad N_F = 357\mu^{-2.44} \tag{1c}$$

The deformation capacity before fracture of SCS is larger than that of SCWB, which also correspond to the order of flexural strength shown in Fig. 7. To investigate the differences of deformation capacity between SCS and SCWB, bending moment carried by beam flange at the first cycle of loading were compared, which was calculated using strain gage pasted on the beam end connection. Bending moment carried by beam flange divided by total bending moment, ${}_bM_f\,/{}_bM$, is shown in Fig. 9. After slippage of beam web-bolted connection, ${}_bM_f\,/{}_bM$ of SCWB was larger than that of SCS, which causes large strain at the beam flange connection and the differences of deformation capacity before fracture.

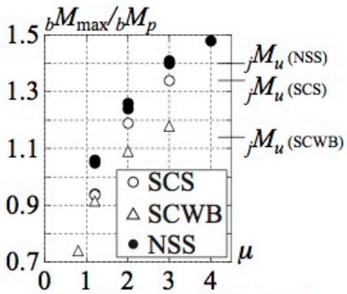

Fig. 7. Flexural Strength

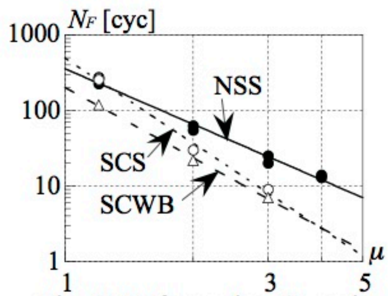

Fig. 8. Deformation Capacity

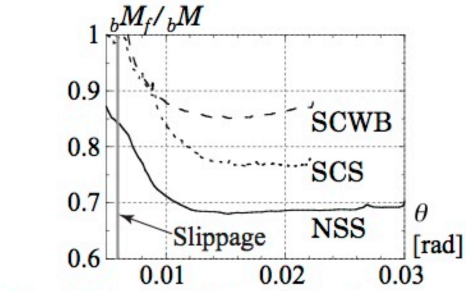

Fig. 9. Burden Ratio of Bending Moment

4. Evaluation Method of Fracture

4.1 Investigation of Crack Propagation Leading to Fracture

From the observation of crack propagations during constant amplitude loading tests, it is confirmed that specimens with weld access holes fractured as a result of crack initiated at the toe of the weld access hole and that specimens without weld access holes fractured as a result of crack initiated at the edge of the CJP weld. Crack-propagation measurements were made as shown in Figs. 10; the results are shown in Figs. 11. The ordinate d is the crack depth for the SCS and SCWB specimens and l is the crack length for the NSS specimens, and the abscissa, n, is the number of cycles, N, normalized by N_F.

From the results in Figs. 11, it is evident that the crack propagation behavior varies depending on type of the connection and the loading amplitude. For all cases, crack propagations can be divided in three stages: (1) no crack is observed, (2) the crack initiation and gradual propagation, (3) rapid propagation to the point of fracture.

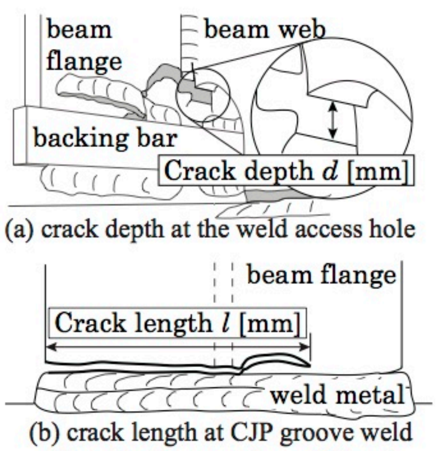

Fig. 10. Observation of Crack

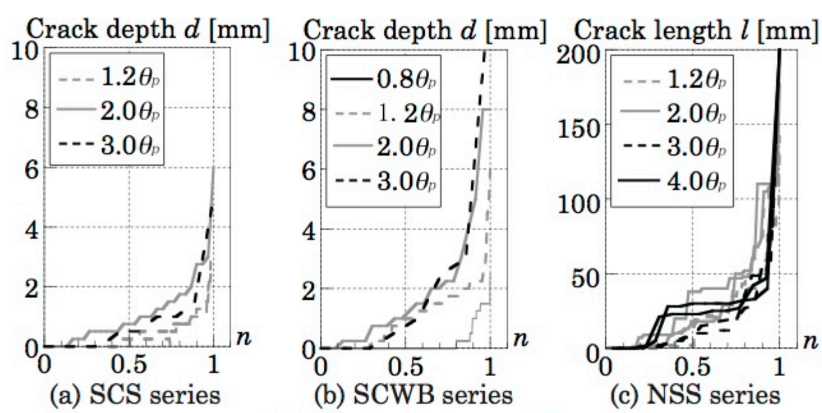

Fig. 11. Crack Propagations Measured at Constant-Amplitude Loading Tests

4.2 Crack Propagation Analysis for Damage Evaluation

To evaluate damage of moment connection before fracture, cracks that led to total fracture were analyzed quantitatively and the crack-propagation curves were plotted. Based on the results in Figs. 11, crack propagation curves were approximated, as shown in Fig. 12. For the specimens without weld access holes, the relationships between the normalized number of cycles, n, and the crack length, l, are formulated as Eqs. 2. In these relationships, n is regarded as the damage index. For the specimens with weld access hole, the relationships between n and the crack depth, d, are formulated.

$$\text{1st stage: } l = 0 \qquad (0 \le n \le n_s) \tag{2a}$$

$$\text{2nd stage: } l = j_2\,(n^3 - n_s^3)\,N_F^3 / 6 \qquad (n_s < n \le n_{F\text{-}1}) \tag{2b}$$

$$\text{3rd stage: } l = v_3\,(n - n_{F-1})\,N_F + l_{F\text{-}1} \quad (n_{F\text{-}1} < n \le 1) \tag{2c}$$

where, n_s, n at the beginning of second stage

j_2, j at the second stage [mm/cyc^3]

$n_{F\text{-}1}$, n at the end of the second stage; $(N_F - 1) / N_F$

$l_{F\text{-}1}$, crack length at the end of the second stage; $j_2\,N_F^3\,(n_{F\text{-}1}^3 - n_s^3) / 6$ [mm]

v_3, v at the third stage; $(l_F - l_{F\text{-}1}) / 1$ [mm/cyc]

l_F, l at fracture [mm]

The number of cycles at the beginning of the second stage is determined by visual observation during loading tests, and the beginning of the third stage is defined as one cycle before total fracture occurs. The coefficients n_s and j_2 are determined from each test result, and the relationships between the ductility amplitude, μ, and these coefficients are shown in Figs. 13. From regression analysis, the coefficients were obtained. n_s is defined as the mean value of the test results and j_2 is considered to have a liner relationship with μ in a double logarithmic plot. The other coefficients, n_{F-1}, l_{F-1} and v_3, are obtained from N_F, n_s and j_2.

The relationships between l and n, and d and n are shown in Figs. 14. These formulated crack -propagation curves are presented as a function of the number of cycles and the deformation amplitude. The differences between these curves indicate that both the presence of a weld access hole and the flexural strength affect on crack propagation.

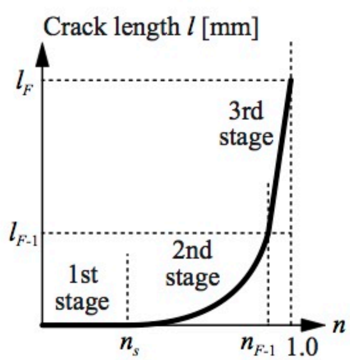

Fig. 12. Crack-Propagation Curve

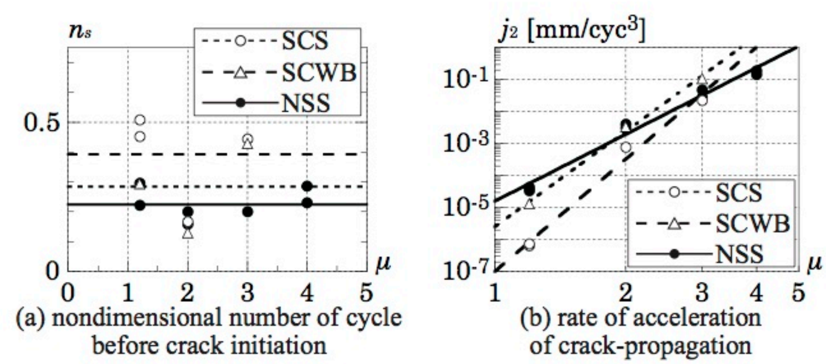

Fig. 13. Coefficients of Crack-Propagation

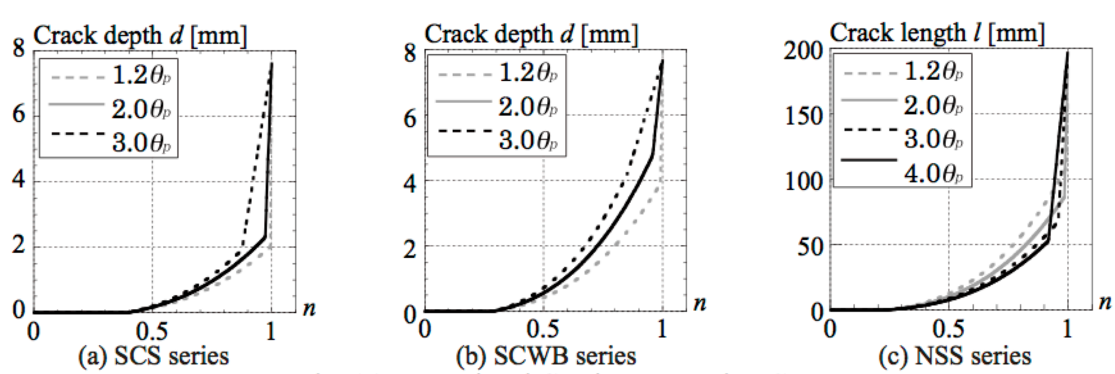

Fig. 14. Formulated Crack-Propagation Curve

5. Verification of Crack Propagation Rule

5.1 Varying-Amplitude Loading Test

To verify the validity of crack propagation rule, two kinds of varying-amplitude loading tests were conducted for SCS and SCWB specimens and the deformation capacity before fracture was investigated. According to the previous study[13], one was two-step constant-amplitude loading tests as the simplest loading protocol, and the other was random-amplitude loading tests simulating the seismic response against long-period ground motions comparable to those predicted for Nankai Trough earthquakes.

In two-step constant-amplitude loading tests, the loading protocol consisted of two different constant amplitudes. The ductility amplitudes of the first and second step are denoted μ_1 and μ_2, and the number of cycles of each step are denoted N_1 and N_2, respectively. Whereas in random-amplitude loading tests, the loading histories were obtained by time history response analysis conducted to simulate the seismic response of the moment connections of tall steel buildings subjected to long-period ground motions. Two steel tall buildings designed according to seismic regulations set in the 1970s and two simulated ground motion for a hypothetical Nankai Trough were used. All varying-amplitude loading histories are shown in Figs. 15.

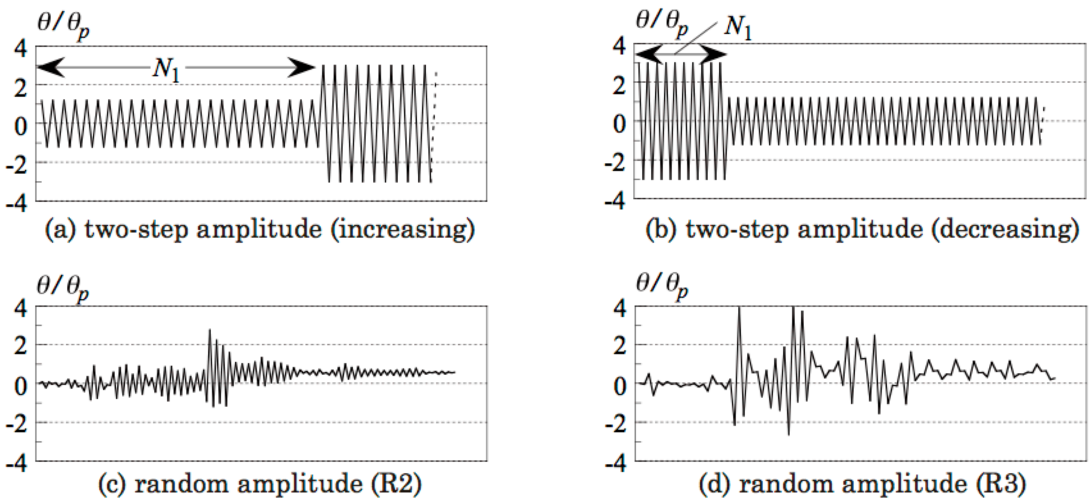

Fig. 15. Varying-Amplitude Loading Histories

For a representative tests, the relationship between the bending moment, $M/{}_bM_p$, and the rotation, θ/θ_p, is shown in Figs. 16. The result from all performed with varying-amplitude cyclic loadings are summarized in Table 4. The damage index of the first step, n_1, is defined as N_1/N_{F1}, where N_{F1} is the number of cycles before fracture under constant cyclic deformation and is calculated by Eq. 1 using the ductility of amplitude μ_1. That of second step, n_2, is also defined as N_2/N_{F2}. D_{exp} is the experimental value of the damage index before fracture, which is the sum of n_1 and n_2 for two-step constant-amplitude loading tests and is the sum of n counted by Rain-flow method for random amplitude loading tests.

From the results of two-step constant-amplitude loading tests in Table 4, the damage index for the increasing-amplitude loading test was smaller than 1.0, and that for the decreasing-amplitude loading test was larger than 1.0. According to Miner's rule, the damage index should be 1.0 for all tests and the deformation capacity should not depend on the direction in which the loading amplitude is changed (that is, increased or decreased). Thus, Miner's rule is not applicable for varying amplitude loading. From the results of random amplitude loading test in Table 4, the loadings were repeated with identical time histories before beam fracture occurred. By the loading R3 with maximum ductility amplitude of 4.0, the minimum number of loading repetitions was 2 for the SCWB and 3 for the SCS specimens. Therefore, these specimens no room on deformation capacity to protect them against long-period ground motions comparable to those predicted for Nankai Trough earthquakes.

A comparison of cumulative plastic deformation, η_F, of SCS, SCWB and NSS is shown in Fig. 17. η_F increases in the order: SCWB<SCS<NSS, which corresponds to the result of constant-amplitude loading tests. These results indicate that against significant cyclic deformation in the plastic range caused by long-period ground motions, the moment connection without weld access hole has higher deformation capacity than those with weld access hole and moment connection with high flexural strength has also high deformation capacity than those with low flexural strength.

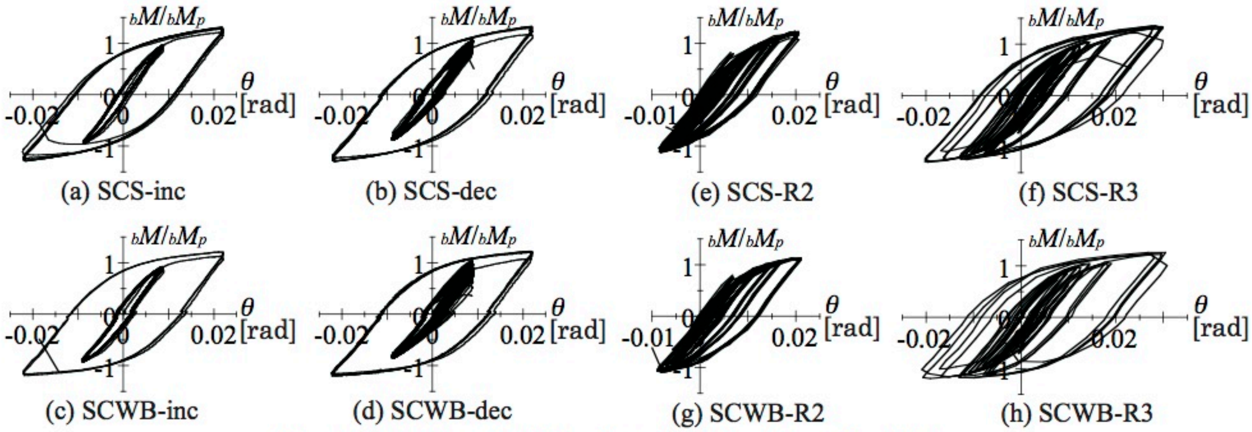

Fig. 16. Results of the Varying-Amplitude Loading Tests

Table 4. Summary of Results from Varying-Amplitude Cyclic Loading Tests

Test Name	Loading History	Number of Loadings	D_{cxp}	η_F
SCS-inc	Fig. 15 (a)	μ_1=1.2 (N_1=52) μ_2=3.0 (N_2=7)	1.08	71.0
SCS-dec	Fig. 15 (b)	μ_1=3.0 (N_1=5) μ_2=1.2 (N_2=151)	1.23	164
SCWB-inc	Fig. 15 (a)	μ_1=1.2 (N_1=58) μ_2=3.0 (N_2=3)	0.938	70.3
SCWB-dec	Fig. 15 (b)	μ_1=3.0 (N_1=4) μ_2=1.2 (N_2=77)	1.25	98.0
SCS-R2	Fig. 15 (c)	Number of repetitions = 16	0.941	157
SCS-R3	Fig. 15 (d)	Number of repetitions = 3	1.25	84.3
SCWB-R2	Fig. 15 (c)	Number of repetitions = 9	1.09	87.1
SCWB-R3	Fig. 15 (d)	Number of repetitions = 2	1.12	56.2

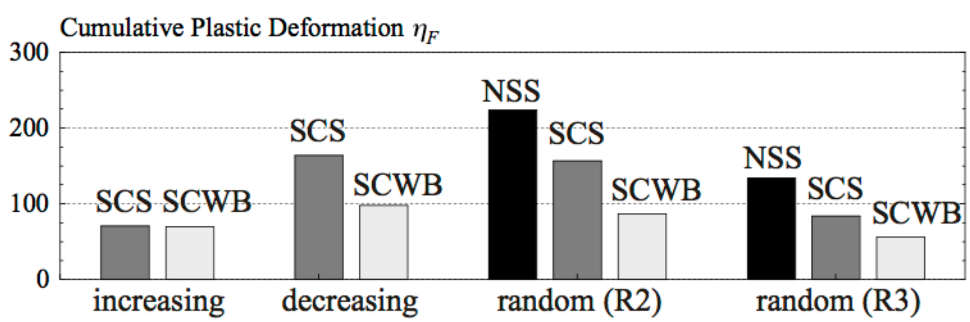

Fig. 17. Results of the Varying-Amplitude Loading Tests

5.2 Estimation of Fracture Using the Crack Propagation Rule

To estimate fracture under loading with varying amplitude, a method to calculate the damage index before fracture is proposed. As shown in Figs. 18, the method involved evaluation of the damage index for two-step constant-amplitude loading. The instance when the crack length reaches l_F (i.e. 200mm) is considered as the point of fracture and the normalized number of cycles, n, is the damage index, D_{cal}. Because the crack-propagation curves differ according to the amplitude, if μ_1 is smaller than μ_2, D_{cal} is smaller than 1.0, whereas if μ_1 is larger than μ_2, D_{cal} is larger than 1.0.

A comparison of the value of D_{cal} and D_{exp} presented in Fig. 19 demonstrates that these are in close agreement. This means that the proposed crack-propagation rule can be used to evaluate the influence of the amplitude (and the direction in which it is varied) and that is more effective than Miner's rule for evaluating the damage index under loadings of varying amplitude. The agreement between the experimental and calculated values demonstrates the validity the of crack-propagation rule.

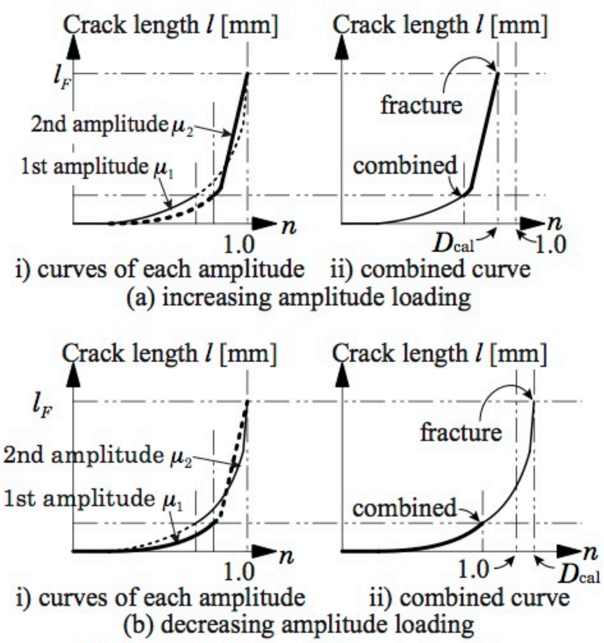

Fig. 18. Method to Estimate Fracture

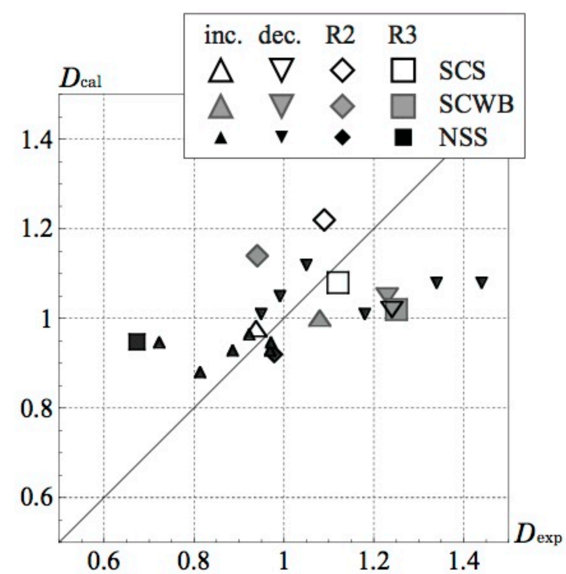

Fig. 19. Comparison of Damage Indexes during Varying-Amplitude Loading Tests

6. Conclusion

To investigate the effect of flexural strength of beam web connection on deformation capacity before fracture and to estimate the point of fracture of moment connections subjected to cyclic plastic deformation, three series of cyclic loading tests were conducted using three types of moment connection with different flexural strength and welding details.

From constant-amplitude loading tests, the effect of flexural strength and the difference of deformation capacity were investigated. Moreover, taking into considering the influence of ductility amplitude on the rate of crack propagation, a crack propagation rule was proposed to evaluate the damage and fracture. The rule was validated by two-step constant -amplitude and random-amplitude cyclic loading tests. The rule was applied to ascertain the effect of the flexural strength of the connection on the deformation capacity for long-period ground motions, such as those predicted for hypotheses Nankai Trough earthquakes. It is also shown that the proposed estimation method well evaluate the instant of fracture and the accuracy of the method is better than Miner rule.

7. Acknowledgements

This research was supported by the Grants-in-Aid for Scientific Research (A) (KAKENHI No.21246087) and Grants-in-Aid for JSPS Fellow (KAKENHI No.25-4696), from Japan Society for the Promotion of Science (JSPS).

8. References

[1] Kasai K., Pu W. C. and Wada A. (2012): Responses of tall buildings in Tokyo during the 2011 Great East Japan Earthquake. *Proceedings of the 7th international conference on STESSA*, 25-35.

[2] Suita K. (2012): Seismic evaluation and retrofit of welded moment connection of early high-rise buildings subjected to long-period ground motions. *Proceedings of the 7th international conference on STESSA*, 1057-1063.

[3] Architecture Institute of Japan (2007): Japanese architectural standard specification JASS 6 steel work (in Japanese).

[4] Suita K. and Tanaka T. (2000): Flexural strength of beam web to square tube column joints. *Steel Construction Engineering*, Japanese Society of Steel Construction, **7** (26), 51-58. (in Japanese)

[5] Campbell S. D., Richard R. M. and Partridge J. E. (2008): Steel moment damage prediction using low-cycle fatigue. *Proceedings of 14th WCEE*, 0255.

[6] Campbell S. D. and Richard R. M. (2012): Cumulative damage model for steel moment frame connection. *Proceeding of the 7th international conference on STESSA*, 221-226.

[7] Amiri A., Rojas F. and Anderson J. C. (2012): Effect of low-cycle fatigue on steel moment frames with RBS. *Proceeding of the 7th international conference on STESSA*, 83-89.

[8] Miner M. A. (1945): Cumulative damage in fatigue. *Journal of Applied Mechanics, Trans. ASME*, **67**, 159-164.

[9] Coffin L. F. (1954): A study of the effects of cyclic thermal stresses on a ductile metal. *Trans. ASME*, **76**, 931-950.

[10] Manson S. S. (1965): A complex subject-some simple approximations. *Experimental Mechanics*, SEM, **5** (4), 193-226.

[11] Zhou. Z, Ito T. and Kuwamura H. (2008): Geometrical and metallurgical notches of welded joints of steel beam-to-column connections Part 5. *Summaries of Technical Papers of Annual Meeting Structures III*, Architecture Institute of Japan, 999-1000 (in Japanese).

[12] Yamada S., Jiao Y. and Kishiki S. (2011): Plastic deformation capacity of steel beam determined by ductile fracture under various loading histories. *Proceeding of Constructional Steel*, Japanese Society of Steel Construction, **19**, 239-246 (in Japanese).

[13] Suita K., Manabe Y., Takatsuka K., Tanaka T. and Tsukada T.: Prediction of Fracture of Steel Moment Connection by Cyclic Loading with Various Deformation Amplitude, *Proceeding pf 15th WCEE*, 2724.